ACS APPLIED MATERIALS & INTERFACES

www.acsami.org

Research Article

Ionic Rectification by Dynamic Regulation of the Electric Double Layer at the Hydrogel Interface

Yaowen Ouyang, Xiang Li, Shaoxin Li, Zhong Lin Wang,* and Di Wei*

Cite This: *ACS Appl. Mater. Interfaces* 2024, 16, 18236−18244

Read Online

ACCESS | Metrics & More | Article Recommendations | Supporting Information

ABSTRACT: Hydrogels play a pivotal role in the realm of iontronics, contributing to the realization of futuristic human−machine interactions. The electric double layer (EDL) between the hydrogel and electrode provides an essential ionic−electronic coupling interface. While prior investigations primarily delved into elucidating the formation mechanism of the EDL, our study shifts the focus to showcasing the current generation through the mechanical modulation of the EDL at the hydrogel−metal interfaces. The dynamic EDL was constructed by the mechano-driven contact−separation process between the polyacrylamide (PAAm) hydrogel and Au. Influencing factors on the dynamic regulation of the EDL such as ion concentration, types of salt, contact−separation frequency, and deformation degree were investigated. Dehydration usually limits the practical applications of hydrogels, and it is a long-standing and difficult problem. However, it seemed to be able to slow the EDL formation process here, resulting in a sustained continuous direct current signal output. Such hydrogel iontronics could rectify the displacement electronic current of a triboelectric nanogenerator by the ionic current. The directional migration of ions could be further enhanced by using charge-collecting metals with different work functions, for example, Au and Al. It offers a paradigm to enable ionic rectification that could be seamlessly incorporated into electronic systems, ushering in a new era for efficient energy harvesting and biomimetic nervous systems.

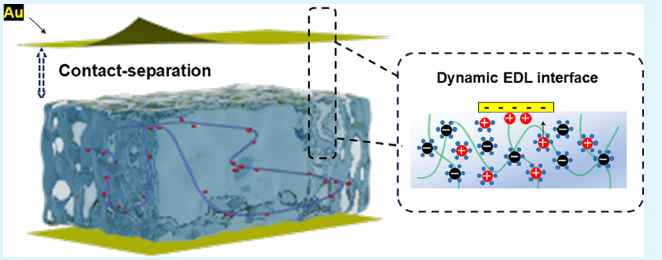

KEYWORDS: *hydrogel iontronics, hydrogel interfaces, dynamic electric double layer, ionic rectification, triboelectric nanogenerator*

1. INTRODUCTION

The transmission of electronic signals occurs through electrons and holes, while living organisms employ various ions for information transmission.[1] Iontronics is an emerging interdisciplinary concept that aims to study ionic−electronic coupling interface for highly efficient bionic information and energy flow,[2−5] covering the integration of multidisciplinary knowledge such as electrochemistry, solid state physics, electrical engineering, and bioelectronics.[6,7] Hydrogel is a commonly used material in iontronics with unique advantages. It is formed by a large number of water molecules wrapped in a 3D polymer network. The polymer network gives the hydrogel a stretchable solid property, and the water molecules make the hydrogel an ionic conductor.[8] In fact, numerous tissues and organs in both animals and plants exhibit hydrogel characteristics, and synthetically engineered hydrogels can possess a polymer network with excellent biocompatibility.[9,10] The polymer network generally does not scatter light, which could make the hydrogel transparent to visible light, similar to the optical properties of water.[11] Based on the combination of these excellent properties, hydrogels can be widely used in artificial muscles,[12] artificial skins,[11] artificial axons,[13] and flexible triboelectric nanogenerators (TENG).[14] They play an important role in elucidating the ionic−electronic coupling interface and has great potential in human−machine interaction interfaces.

The interaction between ions and the solid interface is comprehensively expounded through the framework of the electric double layer (EDL).[15,16] Originating in 1853, the concept of the EDL was initially postulated by Helmholtz,[17] subsequently refined by Gouy and Chapman.[18,19] Stern later amalgamated Helmholtz's model with the Gouy−Chapman framework, introducing the notion of distinct charge regions: the Stern layer and the diffuse layer.[20] The Stern layer results from the close adsorption of hydrated ions onto the charged electrode, while the diffuse layer correlates with the ion concentration (opposite to the electrode polarity), diminishing as the distance from the electrode surface increases. This Gouy−Chapman−Stern EDL model has enjoyed widespread recognition across various disciplines. Beyond the migration of interfacial ions, studies underscore the paramount role of

Received: February 8, 2024
Revised: March 12, 2024
Accepted: March 13, 2024
Published: March 27, 2024

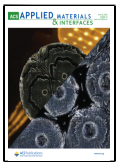

https://doi.org/10.1021/acsami.4c02303
ACS Appl. Mater. Interfaces 2024, 16, 18236−18244

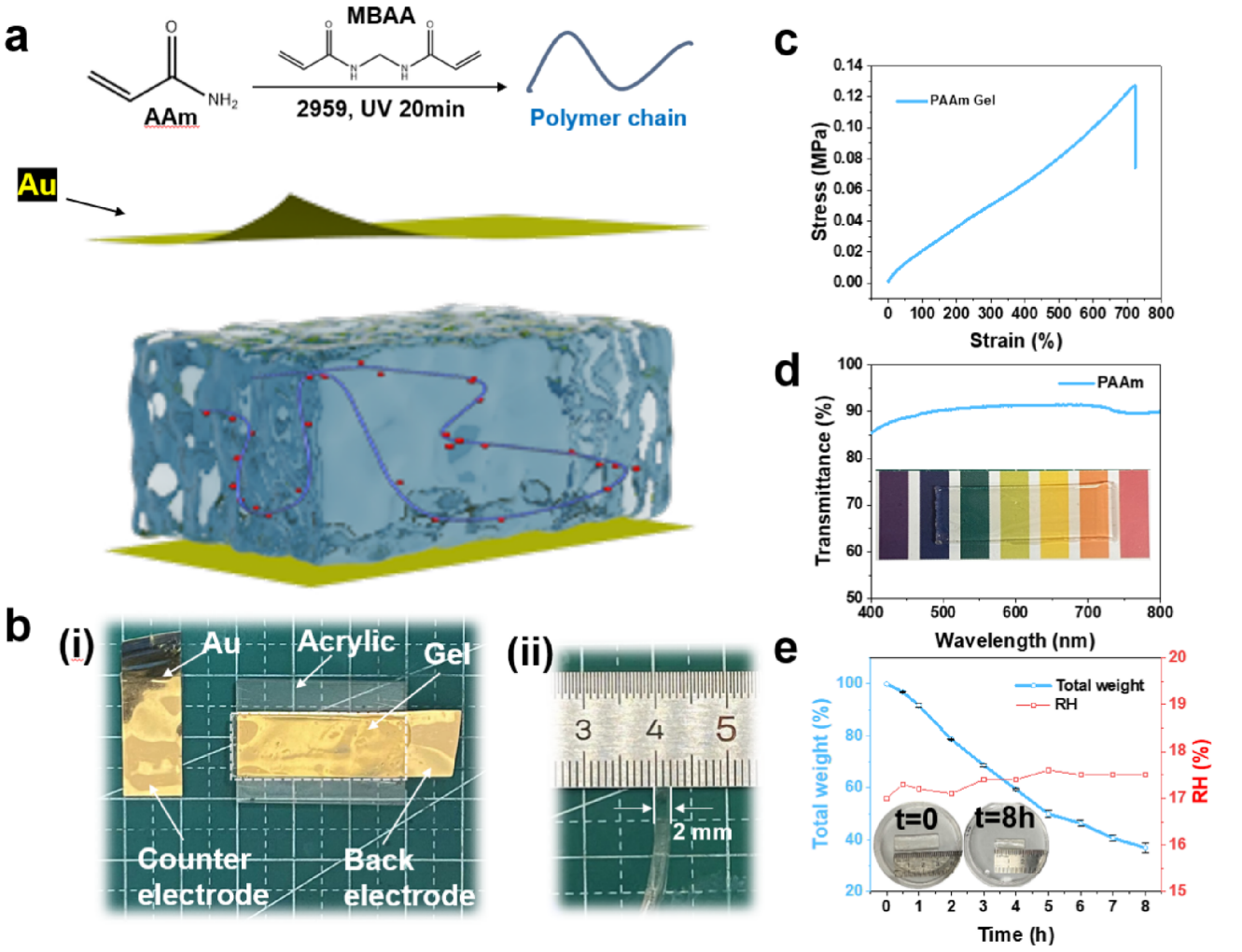

Figure 1. Device structure and hydrogel performance characterization. (a) Theme diagram; (b) photographs showing the structure of this hydrogel device; (c) tensile test of the PAAm hydrogel; (d) transmittance of the hydrogel in the visible light range; (e) PAAm hydrogel dehydration curve (data are mean ± SD, $N = 3$), under an opening room environment.

electron transfer at the solid−liquid contact interface.[21] Wang recently proposed a two-step model to further delineate the EDL formation process for general solid−liquid interface.[22] Past endeavors have been dedicated to the investigation of the static EDL. However, focus of recent advancements is increasingly directed toward probing the dynamics of the EDL process, spurring the emergence of new research paradigms.[23,24] Studies have demonstrated that mechanical stimuli possess the ability to induce alterations in potential by modulating the EDL capacitance or the quantity of charges at the interface, consequently engendering a dynamic current.[25] For example, a TENG based on a hydrogel can modulate the ionic EDL capacitance at the solid−liquid interface by contact electrification (CE) and electrostatic induction. This process facilitates the conversion of mechanical force into electrical energy, empowering self-powered sensors.[26−28] These prior investigations primarily concentrated on the EDL formation between the hydrogel and the dielectric in the TENG. Nevertheless, the ion dynamics within the EDL between metal and hydrogel were disregarded. Understanding ion dynamics within the EDL would open a new scenario in ionic rectification and logic analog, setting a new paradigm in neuromorphic analog and human−machine interface.[24]

This study aims to elucidate the dynamic EDL process induced by mechano-driven interactions between the hydrogel and metal electrode. Gold (Au) was magnetron-sputtered on the PET substrate as the electrode to circumvent the intricate redox reaction processes, maintaining the hydrogel iontronics within the realm of nonfaradaic processes.[9] The contact−separation dynamics between the polyacrylamide (PAAm) hydrogel and Au electrode were systematically investigated. Initially, the PAAm hydrogel (salt-free) and Au electrode were studied as a benchmark, and subsequent analyses delved into the impact of varying concentrations of salt (LiCl) within the PAAm hydrogel. Furthermore, various parameters influencing the dynamic regulation of the EDL, such as salt types, contact−separation frequency, and hydrogel deformation degree, were explored. The dehydration process of hydrogels has perennially posed a limitation on their practical applications. Nonetheless, experiments in this study revealed that the dehydration of PAAm hydrogels in an open environment with low humidity could prove advantageous in inhibiting the rapid formation of the EDL, thereby yielding a durable direct current (DC) signal output. Building upon this observation, an integrated device comprising a hydrogel and a solid−solid contact TENG was conceptualized. The hydrogel demonstrated the ability to rectify the displacement electronic current of the TENG through an

https://doi.org/10.1021/acsami.4c02303
ACS Appl. Mater. Interfaces 2024, 16, 18236−18244

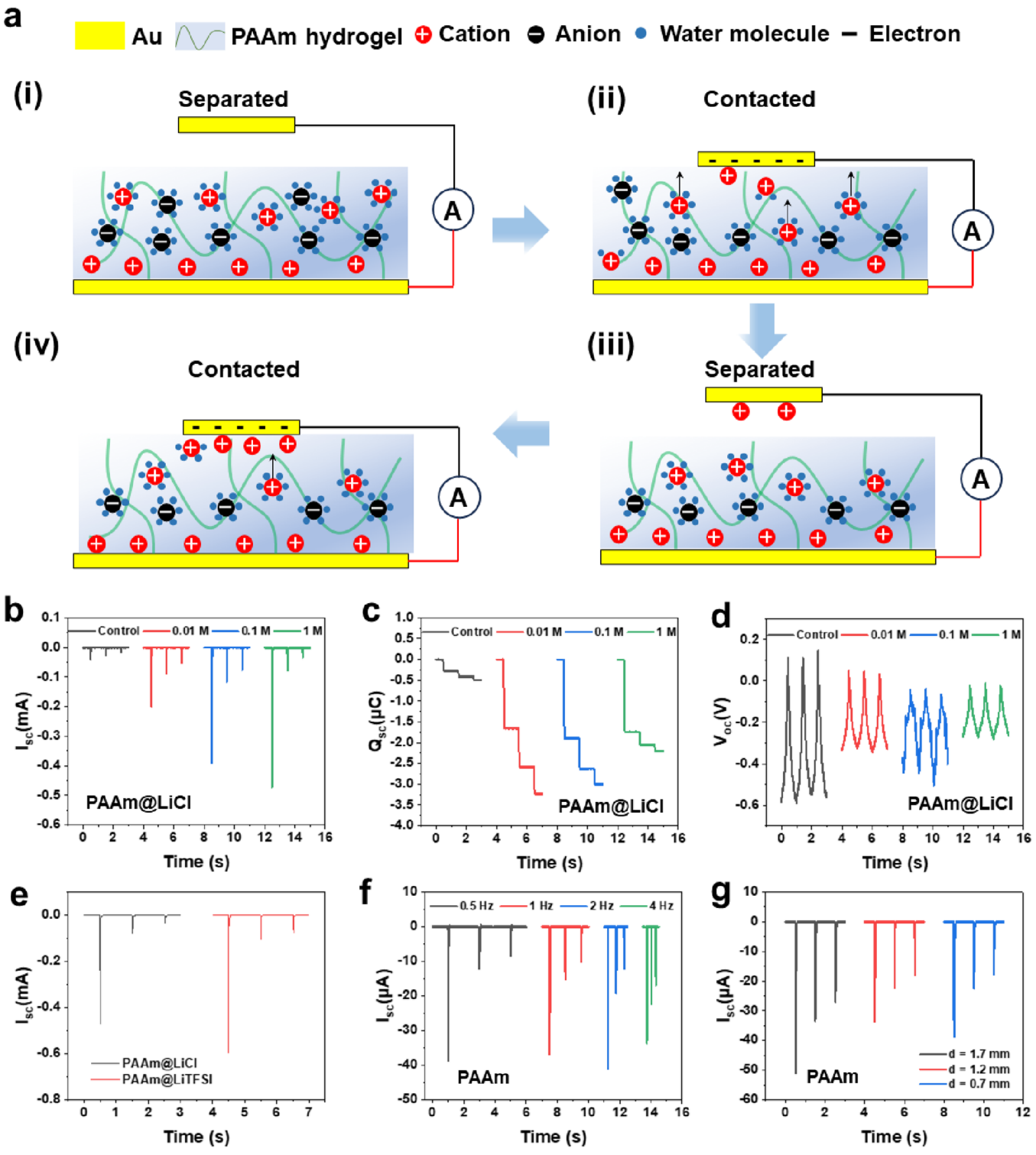

Figure 2. Illustration on dynamic EDL formation and characterization of devices. (a) Schematic diagram of the EDL and ionic current formation mechanism. The effect of the PAAm hydrogel containing different concentrations of LiCl on (b) I_{sc}, (c) Q_{sc}, and (d) V_{oc}; (e) comparison of different kinds of ionic salts (LiCl and LiTFSI) at the same concentration (1 M); (f) influence of different contact−separation frequencies on I_{sc}; (g) effect of different hydrogel deformation degrees on I_{sc}.

ionic current. The directional migration of ions was further augmented by employing charge-collecting metals with distinct work functions, exemplified by Au and Al (with work functions of 5.1 and 4.28 eV, respectively). The hydrogel ion rectifier, conveniently integratable into electronics, presents novel avenues for energy scavenging and human−machine interfaces.

2. MATERIALS AND METHODS

Materials. Acrylamide (AAm, 99%), methylene-bis-acrylamide (MBAA, 99%), 2-hydroxy-4′-(2-hydroxyethoxy)-2-methylpropiophenone (2959), lithium chloride (LiCl, 99%), and bistrifluoromethanesulfonimide lithium (LiTFSI) were all purchased from Macklin and used as received. The Au electrode was prepared by magnetron

https://doi.org/10.1021/acsami.4c02303
ACS Appl. Mater. Interfaces 2024, 16, 18236−18244

sputtering on a polyethylene glycol terephthalate (PET) membrane, the sputtering power was set at 50 W, and the sputtering time was 10 min.

Fabrication of the Hydrogel. AAm (750 mg, monomer), MBAA (7.5 mg, cross-linker), 2959 (50 mg, photoinitiator), and LiCl (42.39 mg) were dissolved in a mixed solvent of D.I. water and ethylene glycol with a total volume of 5 mL (vol:vol = 4:1). Then, it was injected into a self-made acrylic mold and placed under ultraviolet light for 20 min. After curing, it was taken out for the experiment.

Characterization and Measurements. A step motor (Linear Motion 1100) was used to provide the input of mechanical motions. Contact−separation signal data was obtained by using a Keithley electrometer 6514. All electrochemical properties were carried out by an electrochemical workstation (Multi Autolab M204). Electrochemical impedance spectroscopy (EIS) was measured in the range of 0.1 MHz to 1 Hz. Electrochemical experiments related to temperature and RH were performed in an environmental simulation chamber (Vötsch Technik). All high humidity-related experiments were conducted in an environmental simulation chamber controlled by an environmental simulation chamber.

3. RESULTS AND DISCUSSION

PAAm hydrogel synthesis involved the injection of a meticulously prepared reagent solution into a custom-made acrylic mold (Figure S1) and was initiated by ultraviolet light. The Au electrode was fabricated through magnetron sputtering onto a poly(ethylene glycol) terephthalate (PET) substrate. Subsequent to this, various fundamental properties of the hydrogel devices were tested and characterized.

The device structure is depicted in Figure 1a. An asymmetric EDL was established utilizing hydrogel and two Au electrodes to investigate the EDL's role in the dynamic contact−separation process. The test device adopted a sandwich structure, comprising two Au electrodes and a segment of the polyacrylamide (PAAm) hydrogel. The hydrogel's dimensions were 30 mm in length, 10 mm in width, and 2 mm in thickness (Figure 1b). The electrode on the fixed hydrogel side was designated as the back electrode, while the electrode on the hydrogel surface subjected to contact−separation was referred to as the counter electrode. In the experiments detailed in this paper, the effective contact area between the counter electrode and hydrogel was approximately 1 cm^2. The mechanical properties of the hydrogel were assessed through a tensile test. The stress−strain curve revealed a maximum tensile stress of approximately 0.13 MPa and a maximum breaking elongation of 730% (Figure 1c), indicative of the prepared PAAm hydrogel's notable flexibility. Optical transparency was examined through a UV-visible spectrum, and the transmittance of the PAAm hydrogel within the visible light range (wavelength range of 400−800 nm) exceeded 85% (Figure 1d), affirming its good optical transparency. The water retention capacity of the PAAm hydrogel was characterized when exposed openly at room temperature with a stable relative humidity (RH) of approximately 17%. The mass percentage of the hydrogel could be effectively maintained above 90% within approximately 1 h. Extending the duration to 8 h resulted in a decrease of about 40% due to water evaporation (Figure 1e).

The hydrogel constituted a solidified substance engendered by the volumetric augmentation of copious quantities of water within hydrophilic 3D polymer matrices. Evidently, its surface encompasses a profusion of aqueous molecules. Consequently, the EDL at the interface of the hydrogel and the electrode might be reasonably approximated as the interaction between water and the electrode. The selection of Au, an inert metal, was deliberate to preclude redox reactions during the interaction with water. The formation of the EDL and the generation mechanism of the ionic current are shown in Figure 2a. The hydrogel was placed on the back electrode, instigating the establishment of a relatively stable EDL at the interface with the back electrode. At this moment, the counter electrode remained unengaged with the hydrogel, precluding the formation of an EDL at the interface [Figure 2a(i)]. Upon the convergence of the counter electrode with the hydrogel, water molecules facilitated the electron transfer to the counter electrode and then attracted hydrated hydrogen cations, thus giving rise to the EDL [Figure 2a(ii)]. Consequently, a negative current manifested within the external circuit due to the asymmetric EDL between the two electrodes, a phenomenon thoroughly corroborated by subsequent experimental findings. Owing to the robust stability of the EDL adsorption, certain cations persisted on the counter electrode surface postseparation from the hydrogel [Figure 2a(iii)], with this retention accruing through successive contact−separation cycles. Given the finite capacitance of the counter electrode, the establishment of a stable Stern layer signified that the contact−separation process exclusively influenced ion migration within the diffuse layer, potentially eliciting an alternating current (AC) signal [Figure 2a(iv)].

The PAAm hydrogel (salt-free) was used as the control group, and the effects of different concentrations of LiCl within the PAAm hydrogel on the short-circuit current (I_{sc}), transferred charge (Q_{sc}), and open-circuit voltage (V_{oc}) were compared. For the control group (salt-free), the first contact I_{sc} was about 0.04 mA. When the concentration of LiCl increased to 0.01 and 0.1 M, the peak currents of the first contact were 0.2 and 0.4 mA, respectively. As the concentration further increased to 1 M, the peak current did not increase significantly (Figure 2b). The incremental augmentation of I_{sc} was ascribed to the increase in the ion concentration. Upon contact of the Au counter electrode with the hydrogel, rapid ion migration ensued, facilitating the expeditious formation of the EDL. However, the initial contact I_{sc} did not exhibit a linear increase commensurate with the ion concentration, potentially attributable to the constrained capacitance between the electrode and hydrogel interface, signifying a limitation in the adsorption capacity of ions on the Au surface. Consequently, further increments in the ion concentration did not yield a corresponding increase in initial contact I_{sc}. In addition to the initial contact I_{sc}, the attenuation of current during subsequent contact−separation phases might also be ascribed to the swift establishment of the EDL capacitor. The negative charge on the Au electrode underwent partial adsorption and screening by Li^+, diminishing the migration efficacy of Li^+ within the hydrogel. The initial Q_{sc} could also indirectly prove that the capacitance of the EDL interface was limited, with the control group registering approximately 0.25 μC and Q_{sc} escalating to about 1.7 μC at a LiCl concentration of 0.01 M. Moreover, a LiCl concentration increase to 0.1 and 1 M corresponded to a Q_{sc} of approximately 2 μC (Figure 2c). It was worth noting that the current waveform transitions progressively from the DC to AC signal with escalating salt concentration (Figure S2). Upon reaching LiCl concentrations of 0.01 or 0.1 M, the onset of the AC signal manifested around 20 s, whereas a further increase to 1 M reduced the appearance time to approximately 10 s. This transformation in the current waveform from the DC to AC signal might be attributed to the rapid formation of the EDL resulting from augmented free ions and the dense static adsorption of Li^+ on the Au electrode surface. Consequently, the subsequent contact−separation process primarily influenced the oscillatory migration of ions within the diffuse layer. If an EDL was established, then ions

https://doi.org/10.1021/acsami.4c02303
ACS Appl. Mater. Interfaces 2024, 16, 18236−18244

(predominantly Li^+ and H_3O^+) adhered firmly to the Au counter electrode. In accordance with fundamental electrochemistry, the elimination of the EDL was feasible through the application of a reverse voltage, thereby restoring the DC signal. To validate this, upon the appearance of the AC current signal in hydrogel iontronics (Figure S3a), a reverse voltage (0.5 V, 5 mA) was applied for several seconds (10, 20, and 30 s) from an external DC power source. Indeed, the initial contact I_{sc} underwent reconversion to a DC signal (Figure S3b), with the amplitude increasing in proportion to the duration of external power supply application (0.2, 0.22, and 0.47 mA). Although the magnitude of the contact V_{oc} exhibited no significant alteration with the increase in the ion concentration, the induced voltage of the control group surpassed that of the experimental group with LiCl (Figure 2d).

Furthermore, the rate of EDL formation and the duration of the DC signal were tested. Contrary to our initial expectations, the DC signal from the salt-free PAAm hydrogel endured for a minimum of 10 min (Figure S4), whereas the DC duration of the deionized water drop spanned a mere 3−4 min (Figure S5), both under equivalent low humidity and room temperature conditions. In addition to the lower concentration of ions, the protracted establishment of the EDL between the PAAm hydrogel and Au could be elucidated by the comparatively sluggish process. This phenomenon might be attributed to the difference in wettability between the electrode interface and the hydrogel and water droplets. The dehydration of the hydrogel reduced the water content on its surface, and the interfacial wettability between the hydrogel and the counter electrode was poor. Despite the simplification of the EDL transition between the hydrogel and counter electrode into the interaction between water molecules and counter electrode in the previous discourse, the hydrogen bonding involving the polymer and water molecules in the hydrogel demanded consideration when contemplating hydrogel dehydration. Several antecedent investigations have posited that despite hydrogels containing a substantial quantity of water molecules, the physical and chemical characteristics of water within hydrogels differed from those of bulk water molecules owing to the existence of polymer networks.[29] In scrutinizing the physical and chemical processes of hydrogel dehydration, certain models delineated the water within the hydrogel into bound water, intermediate water, and bulk (free) water based on the strength of the hydrogen bond between the polymer network and water (illustrated schematically in Figure S6).[30] Consequently, at low humidity levels, a competitive interplay might ensue between hydrogen bonding and Coulombic interactions as free water on the hydrogel surface is diminished. The former emanated from the polymer network, while the latter arose from the solid−liquid capacitance between water and the counter electrode. This competitive relationship hampered the unimpeded movement of H_3O^+ cations, diminishing the efficiency of EDL formation at the hydrogel−counter electrode interface. To substantiate this hypothesis, elevated humidity levels were implemented in the environmental chamber for validation. Results indicated that at an RH of 60%, the AC signal manifested around 110 s and persisted for the ensuing 5 min. Upon reaching an RH of 90%, the AC signal manifested at approximately 60 s and endured for the following 5 min (Figure S7). These outcomes essentially affirmed that AC signals manifested with increasing humidity, and the time of AC signal occurrence progressively shortened, signifying an augmentation efficiency in EDL formation.

Factors influencing the dynamic regulation of the EDL, such as salt types, contact−separation frequency, and hydrogel deformation degree, were systematically examined. At an equimolar concentration of 1 M for salts, a comparative analysis was performed between LiTFSI and LiCl to elucidate the distinct impacts of varied ionic sizes on salts (Figure 2e). The initial contacts I_{sc} for LiTFSI and LiCl hydrogels was recorded as approximately 0.59 and 0.47 mA, respectively. Nevertheless, the DC signal duration for the LiTFSI hydrogel (Figure S8) surpassed that of Figure S2c. This discrepancy might be ascribed to the larger size of $TFSI^-$ compared to that of Cl^-, inducing spatial volume steric hindrance, thereby hindering the EDL formation process. Subsequent investigation into the contact−separation frequency of the device demonstrated that the initial contact−separation I_{sc} ranged between 35 and 40 μA (Figure 2f). The first maximum Q_{sc} was approximately 0.3 μC (Figure S9a), with the amplitude of the contact V_{oc} ranging from 0.05 to 0.1 V (Figure S9b). These experimental findings seemingly suggested that the device output remained relatively unaffected within a frequency range of 0.5−4 Hz. Additionally, contact−separation frequency testing was conducted on a PAAm hydrogel containing 1 M LiCl. Results indicated that the influence of frequency variations could be negligibly disregarded even with a substantial influx of ions. Due to the significant ion concentration, the initial contact I_{sc} reached approximately 0.3−0.45 mA (Figure S10a), while the first maximum Q_{sc} was around 0.8−1.2 μC (Figure S10b), and the amplitude of the contact V_{oc} ranged from 0.1 to 0.25 V (Figure S10c). Given the flexible nature of the hydrogel material, it became imperative to characterize the impact of deformation on the device performance. Recent investigations have unveiled other mechanisms for the current generation in hydrogels, specifically those propelled by mechano-driven processes such as piezoionic effects.[31,32] The piezoionic effect arises from the disparate migration rates of asymmetric ions. When subjected to external force, anions and cations undergo uneven spatial enrichment, creating an electric field that propels the flow of the electronic current in the external circuit. Nevertheless, within the scope of this study, we posit that the piezoionic effect is not operative. Primarily, the current collection orientation associated with the piezoionic effect is perpendicular to the direction of the external force, whereas the current collection orientation in this study aligns parallel to the external force. Second, the manifestation of the piezoionic effect necessitates external force, and the magnitude of the current exhibits substantial augmentation with increased external force. Experimental validation of hydrogel deformation and current amplitude alterations was undertaken. Au electrodes were deposited onto the PET film via magnetron sputtering, endowing them with a degree of flexibility. A straightforward verification ensued through the gentle contact−separation of the electrode and the hydrogel, as demonstrated in Movie S1. With minimal external force, the contact between the Au electrode and the hydrogel generated an instantaneous current, gradually decaying during subsequent contact−separation, a consistent observation with prior experimental phenomena. Further scrutiny into the impact of deformation on hydrogel devices involved controlling the displacement distance of the motor to modulate the hydrogel's deformation degree. For the salt-free PAAm hydrogel, altering the extrusion distance (defined as "d") from 1.7 to 1.2 and 0.7 mm yielded a negligible change in the initial contact I_{sc}, maintaining levels of approximately 35−50 μA and a contact V_{oc} at about 10−30 mV (Figure S11). Conversely, for the PAAm hydrogel containing 1 M LiCl, the initial I_{sc}

https://doi.org/10.1021/acsami.4c02303
ACS Appl. Mater. Interfaces 2024, 16, 18236−18244

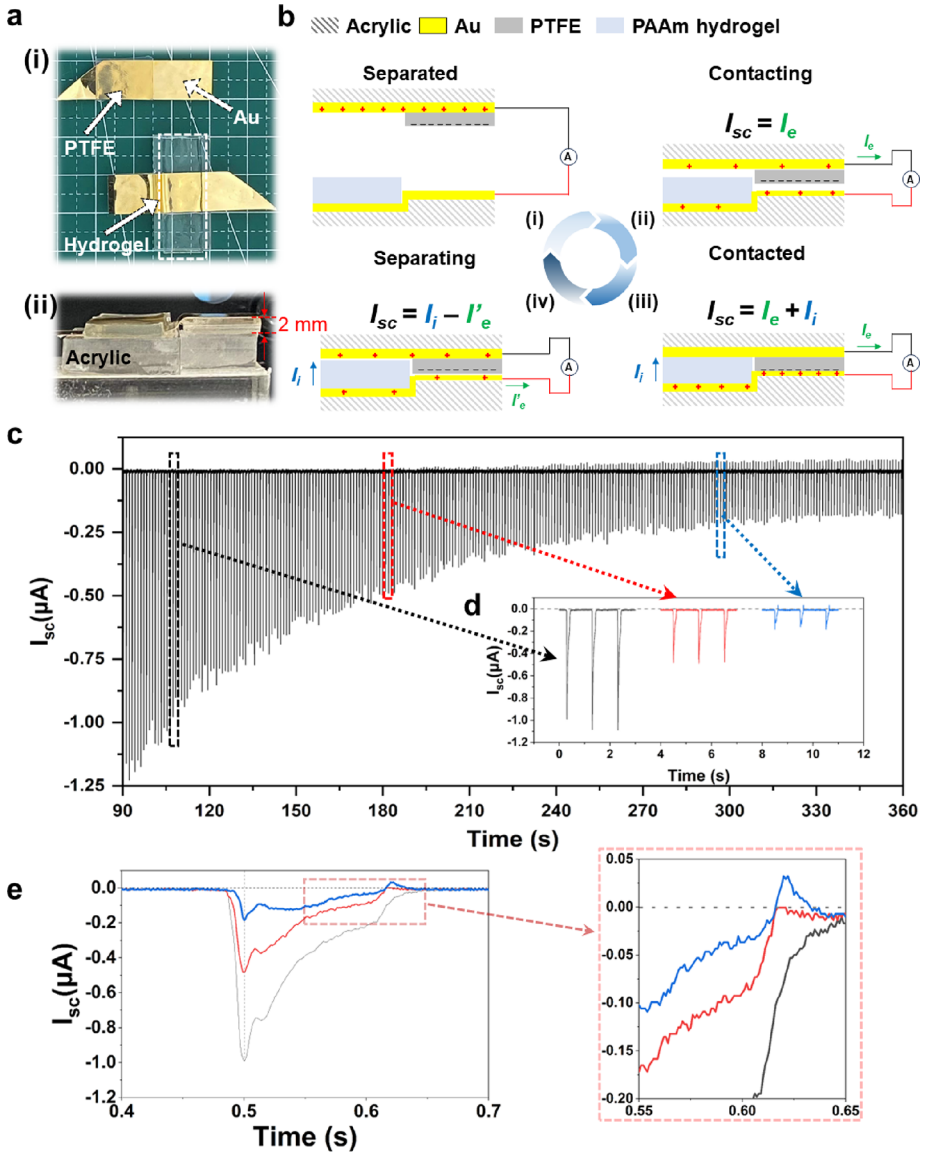

Figure 3. Ionic current used to rectify the electronic current. (a) Structure of the DC-iontronic TENG; (b) rectification mechanism diagram; (c) DC/AC signal transition curve; (d) comparison of current waveforms in different time periods. (e) Single peak current waveform details at different time periods.

corresponding to changes in d (1.7, 1.2, and 0.7 mm) increased from 0.3 and 0.4 to 0.65 mA, respectively (Figure S12a). This phenomenon might be attributed to the decrease in ion resistance stemming from the reduction in d. The contact V_{oc} exhibited a slight increase with decreasing d (Figure S12b). The deformation process was further investigated by assessing the change in the capacitance. For the salt-free PAAm hydrogel, capacitance gradually increased from 1.0 to 2.0 nF with a reduction in d (from 1.7 to 0.7 mm) (Figure S13a). In contrast, for the PAAm hydrogel containing 1 M LiCl (Figure S13b), the capacitance increased from 5.3 to 6.8 μF with a decrease in d (from 1.7 to 1.2 mm). However, further reduction of d to 0.7 mm resulted in capacitance remaining around 6.8 μF, with the effect of continuous d reduction on capacitance being inconsequential.

Upon examination of the robust DC signal from the PAAm hydrogel under low humidity conditions, we harnessed the ionic current emanating from the dynamic EDL interaction between the hydrogel and the Au electrode to rectify the displacement electronic current generated by the TENG. Our preceding investigations have substantiated the efficacy of this approach, demonstrating that the ionic current possessed the ability to counterbalance the electronic current in opposing directions and synergize with the electronic current in parallel.[33] The schematic representation of the integrated device is elucidated in Figure 3a. Acrylic plates served to affix the electrodes, with Au constituting the charge-collecting electrode and PTFE employed as the dielectric substance. The discernible contact area between the hydrogel and the Au electrode amounted to 1 cm^2 [Figure 3a(i)]. Ensuring height consistency between the hydrogel and PTFE, an acrylic plate (2 mm) was utilized to raise the segment of the Au electrode [Figure 3a(ii)]. The mechanism of the ionic current rectifying electronic current is shown in Figure 3b. The working principle of the TENG was based on CE and electrostatic induction effects. PTFE, owing to its higher electronegativity, readily carried a surplus of negative electrons [Figure 3b(i)]. As the counter electrode approached the back electrode, positive charges were induced at the back

https://doi.org/10.1021/acsami.4c02303
ACS Appl. Mater. Interfaces 2024, 16, 18236−18244

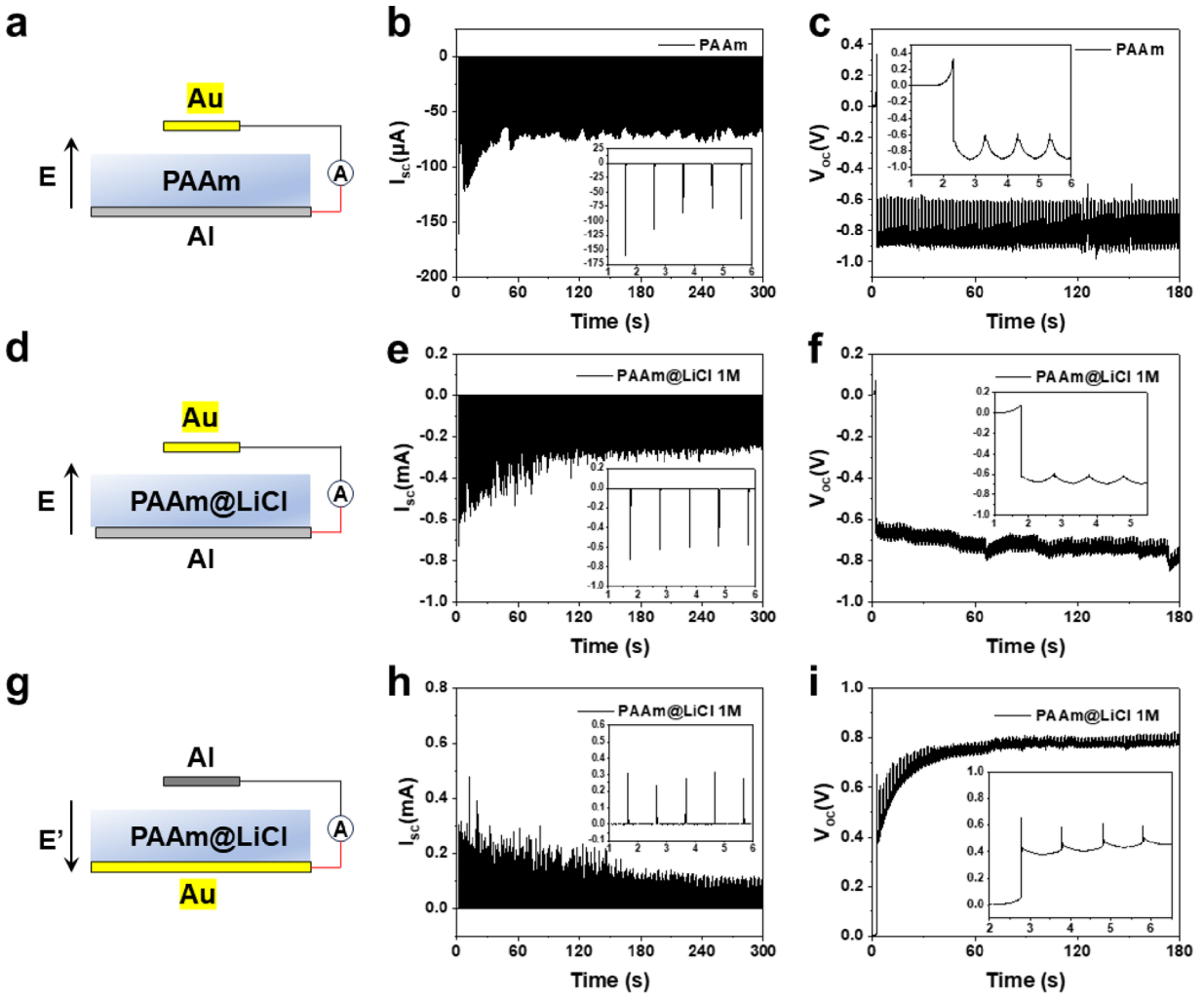

Figure 4. Ion migration modulation regulated by the work function difference electric field. (a) Structure of Au|PAAm|Al, and panels (b, c) refer to its I_{sc} and V_{oc}, respectively. (d) Structure of Au|PAAm@LiCl|Al, and panels (e, f) refer to its I_{sc} and V_{oc}, respectively. (g) Structure of Al|PAAm@LiCl|Au, and panels (h, i) refer to its I_{sc} and V_{oc}, respectively.

electrode through electrostatic induction, thereby generating a negative electronic current (I_e) [Figure 3b(ii)]. Upon closer proximity of the two electrodes, an ionic current manifested and aligned with the electronic current in the same direction [Figure 3b(iii)]. Subsequent separation of the electrodes resulted in the offsetting of the electronic current (I'_e) by the ionic current (I_i), attributed to the faster transport of electrons compared to ions, ensuring prolonged occurrence of the I_i [Figure 3b(iv)]. To validate the feasibility of ionic rectification, the contact−separation test was conducted at room temperature with an RH of 15%, as portrayed in Figure 3c. No discernible positive electronic current was evident before 210 s. However, post the 210 s mark, a positive electronic current gradually emerged concurrent with the decay of the ionic current. Figure S4 illustrates the sustained generation of a DC signal by the PAAm hydrogel for at least 660 s, affirming the role of the ionic current in rectifying the electronic current prior to 210 s, rather than merely capturing the standalone hydrogel current signal. Figure 3d showcases the current waveforms corresponding to different time intervals, with a more conspicuous positive electronic current at 300 s, measuring approximately 45 nA. After removing the hydrogel, the I_{sc} between the PTFE and Au electrode was tested separately. The displacement electronic current at a frequency of 1 Hz was close to 50 nA (Figure S14a), similar to the positive electronic current magnitude measured in Figure 3d. Furthermore, the Q_{sc} (Figure S14b) and the V_{oc} (Figure S14c) at different frequencies exhibited marginal variations, attributed to the difficulty of Au losing electrons. Therefore, the change in frequency could not effectively improve the charge exchange rate between PTFE and Au. The comparative analysis of single current waveforms during distinct time intervals is depicted in Figure 3e. The decrease in ionic current was manifested not only in the attenuation of the current amplitude but also in the contraction of ionic current occurrence duration. When the ionic current diminished to a certain extent, its asynchronous occurrence with the forward electronic current generated by the TENG might emerge as a significant contributor to rectification failure.

Despite the substantial current generated during the contact−separation process between the Au electrode and the hydrogel, the overly low voltage constraints impeded its broader applicability. To address this limitation, we leveraged the variance in the work function of the electrodes to establish an electric field with a controllable direction.[34] This, in turn, facilitated the creation of a more significant potential difference, thereby enabling the controlled migration of ions. As illustrated in Figure 4a, an electrode system comprising Au as the counter electrode, Al as the back electrode, and salt-free PAAm hydrogel

https://doi.org/10.1021/acsami.4c02303
ACS Appl. Mater. Interfaces 2024, 16, 18236−18244

as the medium was constructed. The work functions of Au and Al stand at 5.1 and 4.26 eV, respectively. With a work function difference of 0.8 eV between the two, the calculated theoretical voltage was approximately 0.8 V.[35] Experimental measurements yielded a stable current of about 75 μA (Figure 4b), with a corresponding V_{oc} of approximately 0.8 V, aligning with the theoretical voltage (Figure 4c). To showcase the impact of the ion concentration, Figure 4d employs a hydrogel containing 1 M LiCl as the medium, resulting in a peak current reaching approximately 0.6 mA (Figure 4e). This enhancement could be attributed to the introduction of a substantial number of ions, elevating the ionic conductivity of the hydrogel. Electrochemical impedance spectroscopy (EIS) was employed to assess the ionic resistance of the PAAm hydrogel with varying concentrations of LiCl salts. The Nyquist plot of EIS revealed a charge transfer resistance (Rct) of approximately 1750 Ω for the salt-free PAAm hydrogel, contrasting with an Rct of about 10 Ω for the PAAm hydrogel containing 1 M LiCl (Figure S15). Remarkably, V_{oc} persisted at approximately 0.8 V (Figure 4f). Upon reversing the Au and Al electrodes (Figure 4g) while utilizing the PAAm hydrogel containing 1 M LiCl as the medium, the current direction reversed, and the I_{sc} magnitude measured approximately 0.3 mA (Figure 4h). Concurrently, V_{oc} stabilized at about 0.8 V (Figure 4i). Cyclic voltammetry (CV) curve analysis delineated the direction of the electric field from the side of the Al electrode to the Au electrode, (Figure S16). Linear scanning voltammetry (LSV) experiments comparing the three device structures of Au|PAAm|Au, Al|PAAm|Al, and Au|PAAm|Al demonstrated explicit rectification effects only in the Au|PAAm|Al configuration (Figure S17). Given the susceptibility of the hydrogel to dehydration in an open environment, the endurance of the current under varying humidity conditions was assessed. At low humidity (RH = 30 and 60%), the I_{sc} magnitude experienced significant attenuation, nearly decreasing to below 0.2 mA around the 600 s mark. Conversely, under high humidity conditions (RH = 90%), the I_{sc} durability exhibited minimal attenuation, persisting virtually unchanged even after 7200 s (Figure S18). This underscores the profound influence of the wettability of the hydrogel−electrode interface on the output performance of the device. In this example, the I_{sc} was mainly generated by the electric field constructed by the difference in the work function.

4. CONCLUSIONS

This study elucidates the generation of electricity through mechanical modulation of the dynamic EDL at hydrogel interfaces. The model representing the dynamic EDL was established through a mechano-driven contact−separation process between the PAAm hydrogel and Au electrode. Investigations into the effects of varying ion concentrations, ionic salt types, contact−separation frequencies, deformation degrees, etc., were conducted. As the ion concentration increased, the initial contact I_{sc} magnitude exhibited a rise from 0.04 mA (salt-free) to approximately 0.4 mA (with the ion concentration exceeding 0.1 M), accompanied by a swift transition of the current signal from DC to AC. Interestingly, under low humidity conditions (RH ≤ 20%), the dehydration process of the hydrogel proved advantageous in slowing down the EDL formation, consequently prolonging the output of a DC signal. Conversely, at higher relative humidity levels, the DC signal would transfer to the AC signal more quickly. Under an equivalently high ion concentration (1 M), LiTFSI demonstrated a slower AC signal transition compared to LiCl. The impact of contact−separation frequency on I_{sc}, Q_{sc}, and V_{oc} of the PAAm hydrogel (with and without LiCl) remained inconspicuous within the frequency range of 0.5−4 Hz. While the gradual increase in deformation degree exhibited no apparent effect on the salt-free PAAm hydrogel, it progressively elevated the I_{sc} of the PAAm hydrogel containing LiCl. In low humidity conditions, the integration of the PAAm hydrogel (salt-free) with the conventional solid−solid contact−separation TENG successfully verified the feasibility of ionic current rectification in tandem with the TENG-displaced electronic current. To amplify the ionic current and achieve controllable ion migration, an electric field could also be effectively constructed through the disparity in work function between Au and Al electrodes (5.1 and 4.26 eV, respectively). The present work establishes a paradigm for constructing an ion rectifier seamlessly integratable into electronic systems, potentially opening new avenues for efficient energy harvesting and bionic nervous systems.

■ ASSOCIATED CONTENT

Supporting Information

The Supporting Information is available free of charge at https://pubs.acs.org/doi/10.1021/acsami.4c02303.

Hydrogel preparation mold (Figure S1); the change of the current waveform of PAAm hydrogels absorbing different concentrations of LiCl (Figure S2); EDL removing verification (Figure S3); DC signal duration test of hydrogel and deionized water (Figures S4 and S5); hydrogel dehydration model schematic (Figure S6); DC signal duration test under high humidity (Figure S7); DC signal duration test of the hydrogel absorbed LiTFSI (Figure S8); variable frequency test of nonsalt and salt-containing hydrogels (Figures S9 and S10); the effect of deformation degree on the output of nonsalt and salt-containing hydrogels (Figures S11 and S12); the influence of deformation degree on capacitance change (Figure S13); output of TENG composed of the PTFE and Au electrode (Figure S14); EIS of hydrogels absorbed at different concentrations of LiCl (Figure S15); CV of the hydrogel of the Au and Al electrode system (Figure S16); LSV of hydrogel devices composed of different electrodes (Figure S17); durability test of the hydrogel composed of Au and Al electrodes under different humidities (Figure S18) (PDF)

Video of a gentle contact−separation of the electrode and the hydrogel (MP4)

■ AUTHOR INFORMATION

Corresponding Authors

Zhong Lin Wang − *Beijing Institute of Nanoenergy and Nanosystems, Chinese Academy of Sciences, Beijing 101400, China; Georgia Institute of Technology, Atlanta, Georgia 30332-0245, United States; Guangzhou Institute of Blue Energy, Guangzhou 510555, China;* orcid.org/0000-0002-5530-0380; Email: zhong.wang@mse.gatech.edu

Di Wei − *Beijing Institute of Nanoenergy and Nanosystems, Chinese Academy of Sciences, Beijing 101400, China; School of Nanoscience and Engineering, University of Chinese Academy of Sciences, Beijing 100049, China;* orcid.org/0000-0003-2670-6362; Email: weidi@binn.cas.cn

Authors

Yaowen Ouyang − *Beijing Institute of Nanoenergy and Nanosystems, Chinese Academy of Sciences, Beijing 101400, China; School of Nanoscience and Engineering, University of Chinese Academy of Sciences, Beijing 100049, China*

Xiang Li − *Beijing Institute of Nanoenergy and Nanosystems, Chinese Academy of Sciences, Beijing 101400, China; School of Nanoscience and Engineering, University of Chinese Academy of Sciences, Beijing 100049, China*

Shaoxin Li − *Beijing Institute of Nanoenergy and Nanosystems, Chinese Academy of Sciences, Beijing 101400, China; School of Nanoscience and Engineering, University of Chinese Academy of Sciences, Beijing 100049, China*

Complete contact information is available at: https://pubs.acs.org/10.1021/acsami.4c02303

Author Contributions

D.W. and Z.L.W. proposed the idea and the project. D.W. designed all the experiments and supervised the whole project. Y.O. carried out the experiments in this paper and analyzed the corresponding data. X.L. and S.L. assisted in the experimental testing. All the authors discussed the results and commented on the manuscript. D.W. and Y.O. wrote this paper.

Funding

Beijing Natural Science Foundation (grant no. IS23040)

Notes

The authors declare no competing financial interest.

■ ACKNOWLEDGMENTS

This work was supported by the Beijing Natural Science Foundation (grant no. IS23040).

■ REFERENCES

(1) Chun, H.; Chung, T. D. Iontronics. *Annu. Rev. Anal. Chem.* **2015**, *8*, 441−62.

(2) Someya, T.; Bao, Z.; Malliaras, G. G. The rise of plastic bioelectronics. *Nature* **2016**, *540* (7633), 379−385.

(3) Chen, R.; Canales, A.; Anikeeva, P. Neural Recording and Modulation Technologies. *Nat. Rev. Mater.* **2017**, *2* (2), 1−16.

(4) Lacour, S. P.; Courtine, G.; Guck, J. Materials and technologies for soft implantable neuroprostheses. *Nat. Rev. Mater.* **2016**, *1* (10), 1−14.

(5) Wei, D.; Yang, F.; Jiang, Z.; Wang, Z. Flexible iontronics based on 2D nanofluidic material. *Nat. Commun.* **2022**, *13* (1), 4965.

(6) Bisri, S. Z.; Shimizu, S.; Nakano, M.; Iwasa, Y. Endeavor of Iontronics: From Fundamentals to Applications of Ion-Controlled Electronics. *Adv. Mater.* **2017**, *29* (25), 1607054.

(7) Qian, H.; Wei, D.; Wang, Z. Bionic iontronics based on nano-confined structures. *Nano Res.* **2023**, *16* (9), 11718−11730.

(8) Ahmed, E. M. Hydrogel: Preparation, characterization, and applications: A review. *J. Adv. Res.* **2015**, *6* (2), 105−121.

(9) Yang, C.; Suo, Z. Hydrogel ionotronics. *Nat. Rev. Mater.* **2018**, *3* (6), 125−142.

(10) Lee, Y.; Liu, Y.; Seo, D.-G.; Oh, J. Y.; Kim, Y.; Li, J.; Kang, J.; Kim, J.; Mun, J.; Foudeh, A. M.; Bao, Z.; Lee, T.-W. A low-power stretchable neuromorphic nerve with proprioceptive feedback. *Nat. Biomed. Eng.* **2023**, *7* (4), 511−519.

(11) Keplinger, C.; Sun, J.-Y.; Foo, C. C.; Rothemund, P.; Whitesides, G. M.; Suo, Z. Stretchable, transparent, ionic conductors. *Science* **2013**, *341* (6149), 984−7.

(12) Li, T.; Li, G.; Liang, Y.; Cheng, T.; Dai, J.; Yang, X.; Liu, B.; Zeng, Z.; Huang, Z.; Luo, Y.; Xie, T.; Yang, W. Fast-moving soft electronic fish. *Sci. Adv.* **2017**, *3* (4), No. e1602045.

(13) Yang, C. H.; Chen, B.; Lu, J. J.; Yang, J. H.; Zhou, J.; Chen, Y. M.; Suo, Z. Ionic cable. *Extreme Mech. Lett.* **2015**, *3*, 59−65.

(14) Pu, X.; Liu, M.; Chen, X.; Sun, J.; Du, C.; Zhang, Y.; Zhai, J.; Hu, W.; Wang, Z. L. Ultrastretchable, transparent triboelectric nanogenerator as electronic skin for biomechanical energy harvesting and tactile sensing. *Sci. Adv.* **2017**, *3* (5), No. e1700015.

(15) Parsons, R. Electrical Double-Layer - Recent Experimental and Theoretical Developments. *Chem. Rev.* **1990**, *90* (5), 813−826.

(16) Xu, R.; Shen, X.; Ma, X.-X.; Yan, C.; Zhang, X.-Q.; Chen, X.; Ding, J.-F.; Huang, J.-Q. Identifying the Critical Anion-Cation Coordination to Regulate the Electric Double Layer for an Efficient Lithium-Metal Anode Interface. *Angew. Chem., Int. Ed. Engl.* **2021**, *60* (8), 4215−4220.

(17) Helmholtz, H. Ueber einige Gesetze der Vertheilung elektrischer Ströme in körperlichen Leitern mit Anwendung auf die thierisch-elektrischen Versuche. *Ann. Phys.* **1853**, *165* (6), 211−233.

(18) Gouy, M. Sur la constitution de la charge électrique à la surface d'un électrolyte. *J. Phys. Theor. Appl.* **1910**, *9* (1), 457−468.

(19) Chapman, D. L. LI. A contribution to the theory of electrocapillarity. *Philos. Mag. A* **1913**, *25* (148), 475−481.

(20) Stern, O. Zur Theorie Der Elektrolytischen Doppelschicht. *Z. Elektrochem. Angew. Phys. Chem.* **1924**, *30* (21−22), 508−516.

(21) Lin, S.; Xu, L.; Chi, W. A.; Wang, Z. L. Quantifying electron-transfer in liquid-solid contact electrification and the formation of electric double-layer. *Nat. Commun.* **2020**, *11* (1), 399.

(22) Wang, Z. L.; Wang, A. C. On the origin of contact-electrification. *Mater. Today* **2019**, *30*, 34−51.

(23) Chen, Z. X.; Lu, Y.; Li, R.; Li, D. L.; Xiang, B. L.; Li, J. Q.; Liu, Q. X. Liquid-solid contact electrification through the lens of surface and interface science. *Nano Energy* **2023**, *116*, No. 108834.

(24) Li, X.; Li, S.; Guo, X.; Shao, J.; Wang, Z. L.; Wei, D. Triboiontronics for efficient energy and information flow. *Matter* **2023**, *6* (11), 3912−3926.

(25) Xu, W.; Zheng, H.; Liu, Y.; Zhou, X.; Zhang, C.; Song, Y.; Deng, X.; Leung, M.; Yang, Z.; Xu, R. X.; Wang, Z. L.; Zeng, X. C.; Wang, Z. A droplet-based electricity generator with high instantaneous power density. *Nature* **2020**, *578* (7795), 392−396.

(26) Jia, L.; Guo, Z. H.; Li, L.; Pan, C.; Zhang, P.; Xu, F.; Pu, X.; Wang, Z. L. Electricity Generation and Self-Powered Sensing Enabled by Dynamic Electric Double Layer at Hydrogel-Dielectric Elastomer Interfaces. *ACS Nano* **2021**, *15* (12), 19651−19660.

(27) Yi, F.; Wang, X.; Niu, S.; Li, S.; Yin, Y.; Dai, K.; Zhang, G.; Lin, L.; Wen, Z.; Guo, H.; Wang, J.; Yeh, M.-H.; Zi, Y.; Liao, Q.; You, Z.; Zhang, Y.; Wang, Z. L. A highly shape-adaptive, stretchable design based on conductive liquid for energy harvesting and self-powered biomechanical monitoring. *Sci. Adv.* **2016**, *2* (6), No. e1501624.

(28) Guo, Z. H.; Wang, H. L.; Shao, J.; Shao, Y.; Jia, L.; Li, L.; Pu, X.; Wang, Z. L. Bioinspired soft electroreceptors for artificial precontact somatosensation. *Sci. Adv.* **2022**, *8* (21), No. eabo5201.

(29) Liu, Y.; Liu, X.; Duan, B.; Yu, Z.; Cheng, T.; Yu, L.; Liu, L.; Liu, K. Polymer-Water Interaction Enabled Intelligent Moisture Regulation in Hydrogels. *J. Phys. Chem. Lett.* **2021**, *12* (10), 2587−2592.

(30) Sekine, Y.; Ikeda-Fukazawa, T. Structural changes of water in a hydrogel during dehydration. *J. Chem. Phys.* **2009**, *130* (3), No. 034501.

(31) Dobashi, Y.; Yao, D.; Petel, Y.; Nguyen, T. N.; Sarwar, M. S.; Thabet, Y.; Ng, C. L. W.; Glitz, E. S.; Nguyen, G. T. M.; Plesse, C.; Vidal, F.; Michal, C. A.; Madden, J. D. W. Piezoionic mechanoreceptors: Force-induced current generation in hydrogels. *Science* **2022**, *376* (6592), 502−507.

(32) Li, F.; Cai, X.; Liu, G.; Xu, H.; Chen, W. Piezoionic SnSe Nanosheets-Double Network Hydrogel for Self-Powered Strain Sensing and Energy Harvesting. *Adv. Funct. Mater.* **2023**, 2300701.

(33) Ouyang, Y. W.; Li, X.; Li, S. X.; Peng, P. G.; Yang, F. Y.; Wang, Z. L.; Wei, D. Opto-iontronic coupling in triboelectric nanogenerator. *Nano Energy* **2023**, *116*, No. 108796.

(34) Varpula, A.; Laakso, S. J.; Havia, T.; Kyynäräinen, J.; Prunnila, M. Contacting mode operation of work function energy harvester. *J. Phys. Conf. Ser.* **2014**, *557*, No. 012010.

(35) Varpula, A.; Laakso, S. J.; Havia, T.; Kyynarainen, J.; Prunnila, M. Harvesting vibrational energy using material work functions. *Sci. Rep.* **2014**, *4*, 6799.